Optimal Impulsive Time-Fixed Orbital Rendezvous and Interception with Path Constraints

Article *in* Journal of Guidance Control and Dynamics · February 1990

DOI: 10.2514/3.56656 · Source: NTRS

3 authors, including:

John Prussing
University of Illinois, Urbana-Champaign
90 PUBLICATIONS **1,368** CITATIONS
SEE PROFILE

Victoria Coverstone
University of Miami
78 PUBLICATIONS **1,075** CITATIONS
SEE PROFILE

JOURNAL OF GUIDANCE, CONTROL, AND DYNAMICS
Vol. 18, No. 1, January–February 1995

Optimal Impulsive Time-Fixed Orbital Rendezvous and Interception with Path Constraints

Der-Ren Taur*
Chung Shan Institute of Science and Technology, Lungtan, Taiwan, Republic of China
and
Victoria Coverstone-Carroll† and John E. Prussing‡
University of Illinois at Urbana–Champaign, Urbana, Illinois 61801

Minimum-fuel, impulsive, time-fixed solutions are obtained for the problem of orbital rendezvous and interception with interior path constraints. Transfers between coplanar circular orbits in an inverse-square gravitational field are considered, subject to a circular path constraint representing a minimum or maximum permissible orbital radius. Primer vector theory is extended to incorporate path constraints, and the optimal number of impulses along with their times and positions are determined. The existence of constraint boundary arcs is investigated as well as the optimality of a class of singular arc solutions. A bifurcation phenomenon is discovered in a maximum-radius solution as the transfer time is increased. To illustrate the complexities introduced by path constraints, an analysis is made of optimal rendezvous in field-free space subject to a minimum radius constraint.

Introduction

MOST of the research to date in optimal spacecraft trajectories has considered terminal and time constraints but not interior path constraints.[1–6] Path constraints for impulsive trajectories have been considered by Jezewski and Faust,[7] Jezewski,[8] Brusch,[9] Stern and Fowler,[10] Soileau and Stern,[11] and Prussing and Clifton.[12] These studies contain various conditions to be satisfied for an optimal solution, discussions about path-constrained solutions, and linearized solutions, but no comprehensive solution for a class of path-constrained problems is presented.

The current paper is based mostly on Ref. 13 and considers rendezvous and interception between coplanar circular orbits in an inverse-square gravitational field, subject to a restricted class of interior path constraints, namely, minimum- and maximum-radius constraints. The minimum-radius constraint can be utilized to prevent the spacecraft from colliding with a planet or entering a planet's atmosphere in the case of a planetocentric orbit and to prohibit passing too close to the sun for a heliocentric orbit. Path constraints of this type also have application in maneuvering around large space structures. In a similar manner, a maximum-radius constraint can be used to avoid radiation belts in the planetocentric case and to prohibit venturing too far from the sun for solar panels to be effective in the heliocentric case.

As an introduction to the path-constraint problem, the simple case of optimal transfer between initial and final states at rest in field-free space, subject to a circular interior path constraint is discussed.

Problem Statement

The equations of motion of a spacecraft that is thrusting in a gravitational field on a time interval $0 \leq t \leq T$ can be written in terms of the orbital radius vector $\boldsymbol{r}$ as

$$\dot{\boldsymbol{r}} = \boldsymbol{v} \tag{1}$$

$$\dot{\boldsymbol{v}} = \boldsymbol{g}(\boldsymbol{r}) + \boldsymbol{\Gamma}(t) \tag{2}$$

where $\boldsymbol{\Gamma}$ is the thrust per unit mass, and $\boldsymbol{g}$ is the vector gravitational acceleration. The propellant cost J to be minimized is given by

$$J = \int_0^T \Gamma(t)\, \mathrm{d}t \tag{3}$$

For an n-impulse solution the thrust per unit mass vector is given by

$$\boldsymbol{\Gamma}(t) = \sum_{k=1}^{n} \Delta \boldsymbol{v}_k \delta(t - t_k) \tag{4}$$

where $0 \leq t_1 \leq t_2, \ldots, \leq t_n \leq T$ and each $\Delta \boldsymbol{v}_k$ is the discontinuity in the velocity vector due to a thrust impulse at time t_k, represented by $\delta(t - t_k)$. The cost then reduces to

$$J = \sum_{k=1}^{n} \Delta v_k \tag{5}$$

where the Δv_k are the magnitudes of the discontinuities in the velocity vector. The minimum- or maximum-radius interior path constraint is of the form

$$r(t) \geq r_{\mathrm{mn}} \quad \text{or} \quad r(t) \leq r_{\mathrm{mx}} \tag{6}$$

and is implemented by enforcing a periapse or apoapse radius constraint. Figure 1 shows the geometry for a minimum-radius constraint transfer for which the periapse of the orbit is equal to the constraint radius r_{mn}.

The initial orbit and the rendezvous or interception terminal constraints are specified in terms of a constraint function of the form: $\Psi[\boldsymbol{r}(0), \boldsymbol{v}(0), \boldsymbol{r}(T), \boldsymbol{v}(T)] = \boldsymbol{0}$. With the exception of the interior path constraints of Eq. (6), the formulation is equivalent to that in Ref. 5.

Necessary Conditions

The well-known necessary conditions for an optimal impulsive transfer in the absence of interior path constraints can be expressed in terms of the primer vector[1,2,5,8] as follows.

1) The primer vector satisfies $\ddot{\boldsymbol{p}} = \boldsymbol{G}(\boldsymbol{r})\boldsymbol{p}$, where $\boldsymbol{G}(\boldsymbol{r})$ is the gravity gradient matrix and is continuous with continuous first derivative.

2) The primer vector has magnitude $p \leq 1$ during the transfer with the thrust impulses occurring at those instants for which $p = 1$.

3) At each impulse time the primer vector is a unit vector in the optimal thrust direction.

Presented as Paper 90-2972 at the AIAA/AAS Astrodynamics Conference, Portland, Oregon, Aug. 20–23, 1990; received Sept. 17, 1993; revision received May 27, 1994; accepted for publication July 14, 1994.

*Associate Scientist.
†Assistant Professor, Aeronautical and Astronautical Engineering Department. Member AIAA.
‡Professor, Aeronautical and Astronautical Engineering Department. Fellow AIAA.

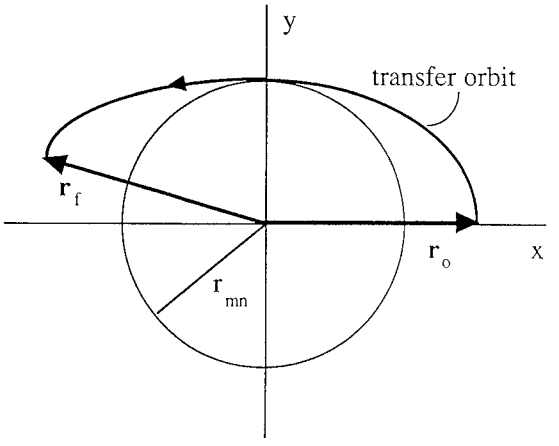

Fig. 1 Orbital geometry for minimum-radius path constraint.

4) As a consequence of condition 2, $\dot{p} = \dot{\boldsymbol{p}}^T \boldsymbol{p} = 0$ at each interior impulse, i.e., at impulse times that are not the initial or final time, the primer magnitude achieves a local maximum value of unity.

With the addition of interior path constraints, these conditions must be modified. A complete description of modifications for multiple-impulse trajectories with and without initial and final coast periods is given in Ref. 13. As a specific example, consider the case in which a midcourse impulse has been added to a two-impulse solution to satisfy a minimum-radius constraint. One then wishes to optimize this three-impulse solution subject to periapse radius constraints on the two coast arcs of the trajectory connecting the three impulses. Gradients of the cost for the constrained problem are derived in the manner of Lion and Handelsman[2] with some generalization. The conditions that cause the gradients of the constrained problem to vanish are then the necessary conditions for an optimal constrained solution.

Consider a three-impulse cost augmented by two periapse constraints, one for each conic segment,

$$\bar{J} = \Delta v_0 + \Delta v_m + \Delta v_f + \lambda_1 \psi_1 + \lambda_2 \psi_2 \tag{7}$$

where the periapse constraints are

$$\psi_1 = r_{\mathrm{mn}} - r_{p_1} \leq 0 \tag{8}$$

$$\psi_2 = r_{\mathrm{mn}} - r_{p_2} \leq 0 \tag{9}$$

where r_{p_1} and r_{p_2} are the periapse radii on the two arcs of the trajectory before and after the midcourse impulse. Apoapse constraints are used to implement maximum-radius constraints in an analogous manner.

Using the symbol $\delta(\,)$ to denote a contemporaneous variation and the symbol $d(\,)$ to denote a noncontemporaneous or skew variation that includes a variation in the time, one examines the variation in the augmented cost $d\bar{J}$ to determine conditions for which $d\bar{J} = 0$, i.e., necessary conditions for a minimum of $\bar{J}$.

$$d\bar{J} = (\dot{\boldsymbol{p}}_m^+ - \dot{\boldsymbol{p}}_m^-)^T d\boldsymbol{r}_m - (H_m^+ - H_m^-) dt_m + \lambda_1 d\psi_1 + \lambda_2 d\psi_2 \tag{10}$$

where the $+$ and $-$ superscripts refer to conditions immediately after and before the thrust impulse, respectively. The terms on the right-hand side of Eq. (10) involving the discontinuity in the primer rate and the Hamiltonian are from the unconstrained problem.[2,5,8] The variations in the constraint functions ψ_k are given by

$$d\psi_1 = \frac{\partial \psi_1}{\partial \boldsymbol{r}_m} d\boldsymbol{r}_m + \frac{\partial \psi_1}{\partial \boldsymbol{v}_m^-} d\boldsymbol{v}_m^- \tag{11}$$

$$d\psi_2 = \frac{\partial \psi_2}{\partial \boldsymbol{r}_m} d\boldsymbol{r}_m + \frac{\partial \psi_2}{\partial \boldsymbol{v}_m^+} d\boldsymbol{v}_m^+ \tag{12}$$

Noting that

$$\dot{\boldsymbol{v}}_m^- = \dot{\boldsymbol{v}}_m^+ = \boldsymbol{g}_m \tag{13}$$

because the position vector is continuous across an impulse, one can use the usual rule relating contemporaneous and noncontemporaneous variations to yield

$$d\boldsymbol{v}_m^- = \delta \boldsymbol{v}_m^- + \boldsymbol{g}_m dt_m \tag{14}$$

$$d\boldsymbol{v}_m^+ = \delta \boldsymbol{v}_m^+ + \boldsymbol{g}_m dt_m \tag{15}$$

The contemporaneous variations in position and velocity are related as in Refs. 2, 5, and 8 using the partitions of the state transition matrix that propagate the state variation $\delta \boldsymbol{x}^T = [\delta \boldsymbol{r}^T \quad \delta \boldsymbol{v}^T]$,

$$\boldsymbol{\Phi}(t_b, t_a) = \begin{bmatrix} \boldsymbol{M}_{ba} & \boldsymbol{N}_{ba} \\ \boldsymbol{S}_{ba} & \boldsymbol{T}_{ba} \end{bmatrix} \tag{16}$$

In particular,

$$\delta \boldsymbol{v}_m^- = \boldsymbol{T}_{m0} \delta \boldsymbol{v}_0^+ \tag{17}$$

$$\delta \boldsymbol{r}_m^- = \boldsymbol{N}_{m0} \delta \boldsymbol{v}_0^+ \tag{18}$$

$$\delta \boldsymbol{v}_m^+ = \boldsymbol{T}_{mf} \delta \boldsymbol{v}_f^- \tag{19}$$

$$\delta \boldsymbol{r}_m^+ = \boldsymbol{N}_{mf} \delta \boldsymbol{v}_f^- \tag{20}$$

In Eqs. (17–20) the fact that $\delta \boldsymbol{r}_0 = \delta \boldsymbol{r}_f = \boldsymbol{0}$ has been used. This is due to the fact that all of the perturbed trajectories start at the same point on the initial orbit at the prescribed initial time and end at the same point and time on the final orbit.

Using the fact that

$$d\boldsymbol{r}_m^\pm = \delta \boldsymbol{r}_m^\pm + \boldsymbol{v}_m^\pm dt_m \tag{21}$$

and Eqs. (17–20) allows $\delta \boldsymbol{v}_m^\pm$ of Eqs. (14) and (15) to be rewritten in terms of $d\boldsymbol{r}_m$ and dt_m as

$$\delta \boldsymbol{v}_m^- = \boldsymbol{T}_{m0} \boldsymbol{N}_{m0}^{-1} [d\boldsymbol{r}_m - \boldsymbol{v}_m^- dt_m] \tag{22}$$

$$\delta \boldsymbol{v}_m^+ = \boldsymbol{T}_{mf} \boldsymbol{N}_{mf}^{-1} [d\boldsymbol{r}_m - \boldsymbol{v}_m^+ dt_m] \tag{23}$$

Substituting Eqs. (22) and (23) along with Eqs. (14) and (15) and (11) and (12) into the expression for $d\bar{J}$ given in Eq. (10) yields the gradients of the augmented cost $\bar{J}$ with respect to $\boldsymbol{r}_m$ and t_m. Equating these gradients to zero yields the necessary conditions for a constrained optimal solution. The gradient with respect to $\boldsymbol{r}_m$ yields

$$\dot{\boldsymbol{p}}_m^{T+} = \dot{\boldsymbol{p}}_m^{T-} - \lambda_1 \frac{\partial \psi_1}{\partial \boldsymbol{r}_m} - \lambda_2 \frac{\partial \psi_2}{\partial \boldsymbol{r}_m} - \lambda_1 \frac{\partial \psi_1}{\partial \boldsymbol{v}_m^-} \boldsymbol{T}_{m0} \boldsymbol{N}_{m0}^{-1} + \lambda_2 \frac{\partial \psi_2}{\partial \boldsymbol{v}_m^+} \boldsymbol{M}_{fm}^T \boldsymbol{N}_{fm}^{-T} \tag{24}$$

where, in the last term of Eq. (24) the symplectic[14] property of the state transition matrix is used to express the partitions that propagate state variations at the final time back to the midcourse time in terms of forward-in-time partitions.

The gradient of the augmented cost with respect to t_m yields another necessary condition

$$H_m^+ = H_m^- + \lambda_1 \frac{\partial \psi_1}{\partial \boldsymbol{v}_m^-} \left[\boldsymbol{g}_m - \boldsymbol{T}_{m0} \boldsymbol{N}_{m0}^{-1} \boldsymbol{v}_m^- \right] + \lambda_2 \frac{\partial \psi_2}{\partial \boldsymbol{v}_m^+} \left[\boldsymbol{g}_m + \boldsymbol{M}_{fm}^T \boldsymbol{N}_{fm}^{-T} \boldsymbol{v}_m^+ \right] \tag{25}$$

The fact that the Hamiltonian is discontinuous is very significant. The periapse constraint is scleronomic, because the time that the trajectory touches the constraint boundary is unconstrained. Furthermore, the time t_m of the midcourse impulse is unconstrained. With no path constraints the Hamiltonian is discontinuous at the midcourse impulse only if the impulse time is constrained.

Because the periapse constraints are inequality constraints the Kuhn-Tucker conditions also require that

$$\lambda_k = \begin{cases} \geq 0 & \text{for} \quad \psi_k = 0 \\ = 0 & \text{for} \quad \psi_k < 0 \end{cases} \tag{26}$$

To relate the periapse constraint functions ψ_k to the conic orbital elements, one uses the fact that in Eqs. (8) and (9)

$$r_{p_k} = a_k(1 - e_k) \tag{27}$$

where a_k and e_k are the semimajor axis and eccentricity, respectively, of the orbit segment k and are given by

$$a_k = \left(\frac{2}{r_m} - v_m^{2\pm}\right)^{-1}; \quad e_k = \left|\left(v_m^{2\pm} - \frac{1}{r_m}\right)\boldsymbol{r}_m - \left(\boldsymbol{r}_m^T\boldsymbol{v}_m^{\pm}\right)\boldsymbol{v}_m^{\pm}\right| \tag{28}$$

where the $-$ superscript is used for segment k and the $+$ is used for segment $k+1$.

In terms of a_k and e_k the expressions for the gradients of the constraint functions appearing in Eqs. (24) and (25) can be written for $e_k \neq 0$ as

$$\frac{\partial\psi_k}{\partial\boldsymbol{r}_m} = \left[\frac{2r_{\mathrm{mn}}a_k}{r_m^3} + \frac{a_k}{e_k}\left[\frac{\sigma_k^2}{r_m^3} - v_m^{2\pm}\left(v_m^{2\pm} - \frac{1}{r_m}\right)\right]\right]\boldsymbol{r}_m^T - \frac{\sigma_k}{e_k}\boldsymbol{v}_m^{T\pm} \tag{29}$$

and

$$\frac{\partial\psi_k}{\partial\boldsymbol{v}_m^{\pm}} = \left(2r_{\mathrm{mn}}a_k + \frac{a_k}{e_k}\left[\sigma_k^2 - 2r_m\left(r_m v_m^{2\pm} - 1\right)\right]\right)\boldsymbol{v}_m^{T\pm} - \frac{\sigma_k}{e_k}\boldsymbol{r}_m^T \tag{30}$$

where

$$\sigma_k \equiv \boldsymbol{r}_m^T\boldsymbol{v}_m^{\pm} \tag{31}$$

For $e_k = 0$ the gradients simplify to

$$\frac{\partial\psi_k}{\partial\boldsymbol{r}_m} = \frac{2}{r_{\mathrm{mn}}}\boldsymbol{r}_m^T \tag{32}$$

and

$$\frac{\partial\psi_k}{\partial\boldsymbol{v}_m^{\pm}} = 2r_{\mathrm{mn}}^2\boldsymbol{v}_m^{T\pm} \tag{33}$$

Field-Free Space

A very simple problem helps to illustrate the complexities of interior path constraints. Consider a fixed-time impulsive rendezvous in field-free space subject to a minimum-radius constraint of the form of Eq. (6) with $r_{\mathrm{mn}} = 1$. As shown in Fig. 2 the vehicle is initially at rest at position $(a, 0, 0)$. The final state is at rest at position $(-a, 0, 0)$. A minimum of three impulses is required to satisfy the boundary conditions subject to the path constraint.

The coast trajectories between impulses are straight lines, and any two line segments connecting the initial and final positions with no portion of the trajectory violating the constraint constitute a feasible solution. Based on the gradients in Eq. (10) the optimal solution can

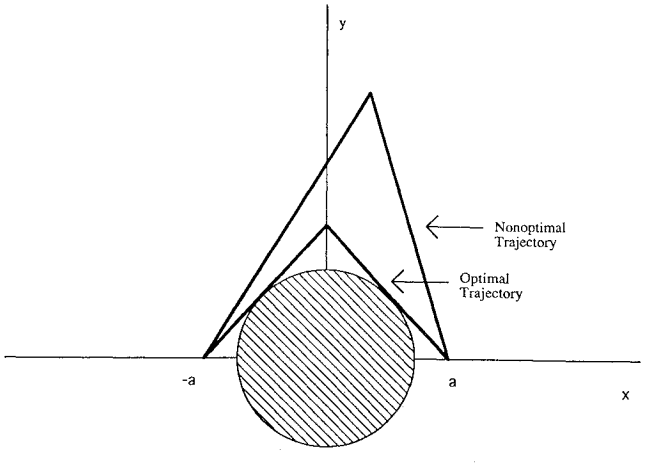

Fig. 2 Optimal and nonoptimal three-impulse field-free solutions.

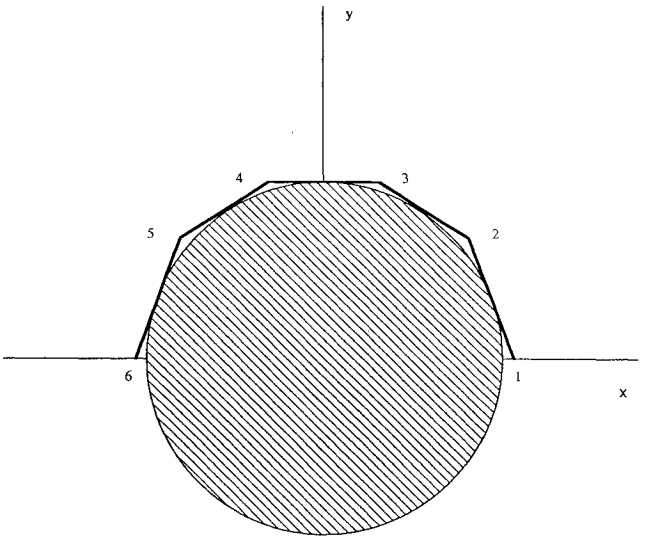

Fig. 3 Optimal six-impulse field-free solution.

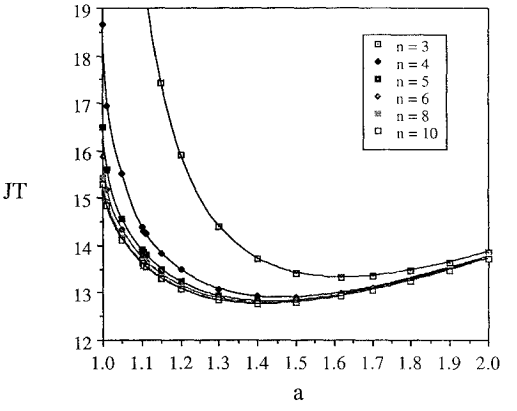

Fig. 4 Optimal field free JT vs number of impulses and initial position.

be shown analytically to consist of the two lines that are tangent to the constraint, with the midcourse impulse on the y axis at time $T/2$ as shown in Fig. 2.

This solution makes physical sense for two reasons: 1) The shorter the distance traveled in a given time, the lower the cost, and the optimal solution minimizes the total distance traveled. 2) On the optimal solution the required rotation of the velocity vector at the midcourse impulse is minimized.

The gradient vector of the cost with respect to the midcourse impulse position, $\dot{\boldsymbol{p}}_m^+ - \dot{\boldsymbol{p}}_m^-$, on the optimal solution lies along the positive y axis, indicating that the only way to reduce the cost is to violate the constraint. For the field-free space case it turns out that the Hamiltonian is continuous across the midcourse impulse, because all of the terms in Eq. (26) contributing to the discontinuity sum to zero.

The cost of the optimal three-impulse solution is

$$J = \frac{4a}{T}\left[\frac{a+1}{a-1}\right]^{\frac{1}{2}} \tag{34}$$

The fact that the product JT is a constant for a given value of a allows one to study the structure of the optimal solutions for different a values, knowing that the cost always decreases with increasing T and that there exists no time-open optimal solution. The dependence of JT on a is somewhat complex. It is not a monotonically increasing function of a but, in fact, has a minimum value. The minimum cost occurs for a value of a that is the root of $a^2 - a - 1 = 0$ equal to $\frac{1}{2}(\sqrt{5}+1) = 1.618$, the so-called golden mean.

Another aspect of the optimal solution is the dependence of the cost on the number of impulses; n-impulse solutions are sufficiently complex to require numerical solution using nonlinear programming. The optimal solution consists of $n-1$ line segments all

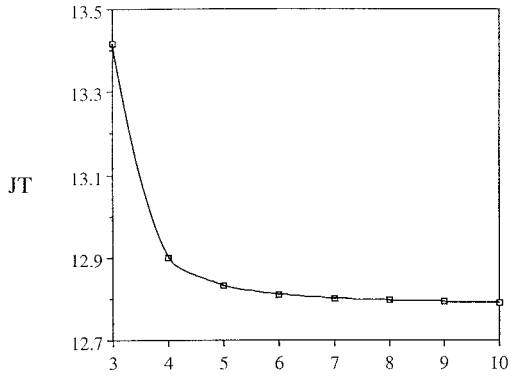

Fig. 5 Optimal field free JT vs number of impulses for $a = 1.5$.

tangent to the constraint with the impulse positions and times optimized by the nonlinear programming algorithm. The optimal six-impulse solution is shown in Fig. 3.

One characteristic of the n-impulse solution is that the cost decreases as the value of n increases. This is shown in Figs. 4 and 5. Also shown in Fig. 4 is that for each value of n there is a minimizing value of a that decreases as n increases. As seen in Fig. 5 the cost asymptotically approaches a minimum value as n increases.

Inverse-Square Gravitational Field

Numerical results are presented for various interior path-constrained problems. Unless otherwise indicated, the initial and target orbits are circular and coplanar. The solutions presented are from Ref. 13 and were obtained using the gradients described and a nonlinear programming algorithm. All numerical values are expressed in canonical units, for which a vehicle in a unit radius circular orbit has unit velocity and an orbital period of 2π canonical time units. The conic orbits are described in terms of universal variables,[14,15] which allow hyperbolic arcs for sufficiently short times between impulses.

Multiple-Impulse Periapse-Constrained Rendezvous

As an example of rendezvous between circular orbits, consider the boundary conditions

$$\boldsymbol{r}_0 = (1.2, 0, 0) \qquad \boldsymbol{r}_f = (-1.961512, -0.3914, 0)$$

To compare the numerical and theoretical (subscript th) results, two three-impulse solutions are shown for two different transfer times.

For $T = 4.35$:

$$\lambda_1 = 0 \qquad \lambda_2 = 0.215907$$

$$\dot{\boldsymbol{p}}_m^+ - \dot{\boldsymbol{p}}_m^- = (0.09529, 0.16337, 0) \qquad H_m^+ - H_m^- = 0.009118$$

$$[\dot{\boldsymbol{p}}_m^+ - \dot{\boldsymbol{p}}_m^-]_{\text{th}} = (0.09529, 0.16338, 0) \qquad [H_m^+ - H_m^-]_{\text{th}} = 0.00912$$

For $T = 3.0$:

$$\lambda_1 = 2.77872 \qquad \lambda_2 = 2.31001$$

$$\dot{\boldsymbol{p}}_m^+ - \dot{\boldsymbol{p}}_m^- = (0.24757, 2.7103, 0) \qquad H_m^+ - H_m^- = -0.28879$$

$$[\dot{\boldsymbol{p}}_m^+ - \dot{\boldsymbol{p}}_m^-]_{\text{th}} = (0.24757, 2.7103, 0) \qquad [H_m^+ - H_m^-]_{\text{th}} = -0.28879$$

Note that the value of $\lambda_1 = 0$ for $T = 4.35$ means that the transfer time is sufficiently long that the periapse constraint on the first conic arc is inactive. For $T = 3.0$ both periapse constraints are active, and the algebraic signs on the Lagrange multipliers satisfy Eq. (26).

For a transfer time $T = 3.0$ the reference cost of the two-impulse solution that violates the minimum-radius constraint of $r_{\text{mn}} = 1$ is 1.404272. Figure 6 shows the cost of the n-impulse periapse-constrained rendezvous solutions for this case as a function of n. Note that the cost is minimized by six impulses.

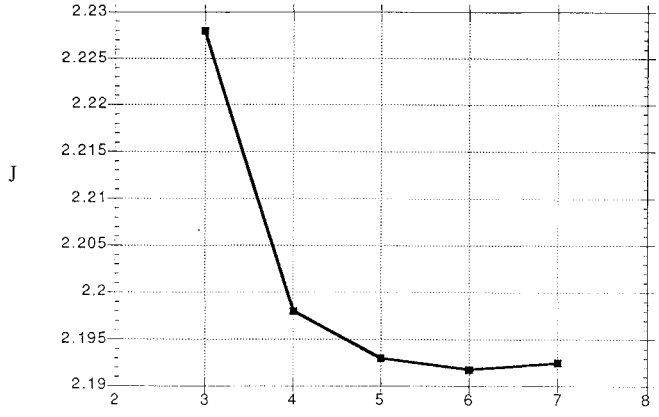

Fig. 6 Optimal rendezvous cost vs number of impulses for $T = 3.0$.

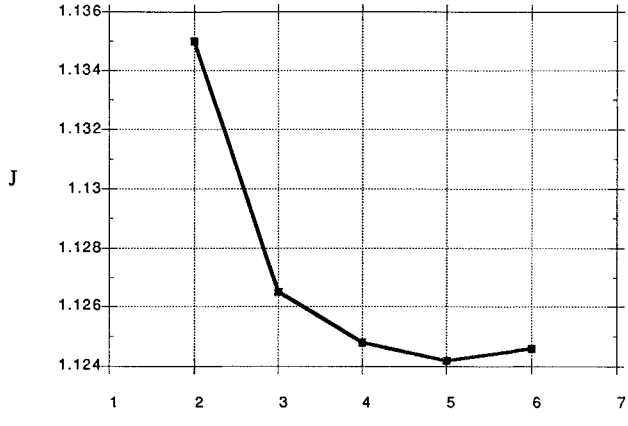

Fig. 7 Optimal interception cost vs number of impulses for $T = 3.0$.

For the $n = 6$ case the optimal solution is as follows:

$$t_1 = 0 \qquad \boldsymbol{r}_1 = \boldsymbol{r}_0$$

$$t_2 = 0.947434 \qquad \boldsymbol{r}_2 = (0.466977, 0.888042, 0)$$

$$t_3 = 1.14013 \qquad \boldsymbol{r}_3 = (0.228673, 0.977201, 0)$$

$$t_4 = 1.32119 \qquad \boldsymbol{r}_4 = (-0.019905, 1.00366, 0)$$

$$t_5 = 1.48958 \qquad \boldsymbol{r}_5 = (-0.2652, 0.968785, 0)$$

$$t_6 = 3.0 \qquad \boldsymbol{r}_6 = \boldsymbol{r}_f$$

$a_1 = 2.84521$	$e_1 = 0.64853$	$\lambda_1 = 1.57065$
$a_2 = 3.98284$	$e_2 = 0.74892$	$\lambda_2 = 0.459554$
$a_3 = 11.29956$	$e_3 = 0.9115$	$\lambda_3 = 0.464761$
$a_4 = -5.886$	$e_4 = 1.16989$	$\lambda_4 = 0.357482$
$a_5 = -1.64764$	$e_5 = 1.60693$	$\lambda_5 = 1.53704$

Note that on the fourth and fifth conic arcs of the six-impulse solution, the time intervals are short enough to require hyperbolic arcs.

Multiple-Impulse Periapse-Constrained Interception

As an example of interception starting from a circular orbit, consider the boundary conditions

$$\boldsymbol{r}_0 = (1.2, 0, 0) \qquad \boldsymbol{r}_f = (-1.961512, -0.3914, 0)$$

For a transfer time $T = 3.0$ the reference cost of the one-impulse solution that violates the minimum-radius constraint of $r_{\text{mn}} = 1$ is 0.717693. Figure 7 shows the cost of the n-impulse periapse-constrained intercept solutions for this case as a function of n. Note

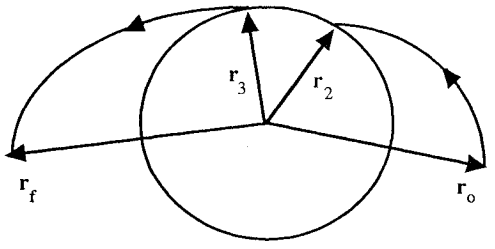

Fig. 8 Four-impulse solution with boundary arc.

that the cost is minimized by five impulses. As one would expect the interception cost shown in Fig. 7 is significantly less than the rendezvous cost in Fig. 6 for the same boundary conditions.

For the $n = 5$ case the optimal solution is as follows:

$$t_1 = 0 \qquad \boldsymbol{r}_1 = \boldsymbol{r}_0$$

$$t_2 = 1.22942 \qquad \boldsymbol{r}_2 = (0.283992, 0.960819, 0)$$

$$t_3 = 1.41235 \qquad \boldsymbol{r}_3 = (0.063119, 1.00036, 0)$$

$$t_4 = 1.57666 \qquad \boldsymbol{r}_4 = (-0.15365, 0.99085, 0)$$

$$t_5 = 1.72122 \qquad \boldsymbol{r}_5 = (-0.36037, 0.93660, 0)$$

$$a_1 = 1.61168 \qquad e_1 = 0.37953 \qquad \lambda_1 = 1.33248$$

$$a_2 = 2.03561 \qquad e_2 = 0.50875 \qquad \lambda_2 = 0.26373$$

$$a_3 = 3.96394 \qquad e_3 = 0.74773 \qquad \lambda_3 = 0.20895$$

$$a_4 = -5.27199 \qquad e_4 = 1.18968 \qquad \lambda_4 = 0.14521$$

$$a_5 = -0.86106 \qquad e_5 = 2.16136 \qquad \lambda_5 = 1.1728$$

Note that all of the λ_k corresponding to active constraints are positive and satisfy Eq. (26). Two of the conic arcs in the optimal solution are hyperbolic, due to the short time interval between impulses.

Boundary Arc Solutions

A boundary arc is a circular arc that lies directly on the constraint boundary. To investigate whether a boundary arc might be part of an optimal constrained multiple-impulse orbit-to-orbit solution, a four-impulse rendezvous with the following constraints at the two midcourse impulse times labeled t_2 and t_3 are imposed for use by the nonlinear programming algorithm.

$$S_1 = \tfrac{1}{2}\left(r_{\text{mn}}^2 - \boldsymbol{r}_2^T\boldsymbol{r}_2\right) \le 0 \tag{35}$$

$$\psi_1 = \boldsymbol{r}_2^T\boldsymbol{v}_2^- \le 0 \tag{36}$$

$$\psi_2 = -\boldsymbol{r}_2^T\boldsymbol{v}_2^+ \le 0 \tag{37}$$

$$S_2 = \tfrac{1}{2}\left(r_{\text{mn}}^2 - \boldsymbol{r}_3^T\boldsymbol{r}_3\right) \le 0 \tag{38}$$

$$\psi_3 = \boldsymbol{r}_3^T\boldsymbol{v}_3^- \le 0 \tag{39}$$

$$\psi_4 = -\boldsymbol{r}_3^T\boldsymbol{v}_3^+ \le 0 \tag{40}$$

Figure 8 shows the geometry for a boundary arc.

The results for two rendezvous and two interceptions are given next. Both the initial and target orbits are circular. The reference cost cited is for the trajectory that violates the minimum-radius constraint. The optimal solution is a four-impulse trajectory with cost given by J_4.

For a rendezvous with $T = 5.1$

$$\boldsymbol{r}_0 = (0.848528, 0.848528) \qquad \boldsymbol{r}_f = (-0.848528, -0.848528)$$

$$J_{\text{ref}} = 0.183623 \qquad \boldsymbol{v}_f = (0.645497, -0.645497)$$

$$J_{\text{boundary-arc}} = 0.325632 \qquad J_4 = 0.239532$$

For a rendezvous with $T = 4.2$

$$\boldsymbol{r}_0 = (0.848528, 0.848528) \qquad \boldsymbol{r}_f = (-0.848528, -0.848528)$$

$$J_{\text{ref}} = 0.400192 \qquad \boldsymbol{v}_f = (0.645497, -0.645497)$$

$$J_{\text{boundary-arc}} = 3.45911 \qquad J_4 = 1.697043$$

For an interception with $T = 5.1$

$$\boldsymbol{r}_0 = (0.848528, 0.848528) \qquad \boldsymbol{r}_f = (-0.848528, -0.848528)$$

$$J_{\text{ref}} = 0.091812 \qquad \boldsymbol{v}_f = (0.645497, -0.645497)$$

$$J_{\text{boundary-arc}} = 0.201022 \qquad J_4 = 0.134149$$

For an interception with $T = 4.2$

$$\boldsymbol{r}_0 = (0.848528, 0.848528) \qquad \boldsymbol{r}_f = (-0.848528, -0.848528)$$

$$J_{\text{ref}} = 0.200096 \qquad \boldsymbol{v}_f = (0.645497, -0.645497)$$

$$J_{\text{boundary-arc}} = 2.358999 \qquad J_4 = 1.21567$$

Note that for both the rendezvous and interception, the cost increases as the transfer time is decreased, as expected. For the same boundary conditions the interception cost is significantly lower than the rendezvous cost, also as expected. However, the most significant result is that, unlike the singular arc case discussed later, the cost on the boundary arc solution is much higher than the four-impulse periapse-constrained solution.

Another significant fact is that the boundary-arc solutions satisfy the necessary conditions for a constrained optimal solution and are, therefore, local optimal solutions. However, the periapse-constrained solutions are also optimal, but with significantly lower costs.

Initial and Final Coast Solutions

Consider a case in which the vehicle is initially in circular orbit on the minimum-radius constraint boundary. The reference solution violates the constraint, and the primer vector magnitude exceeds unity immediately after the initial impulse, indicating that an initial coast would lower the cost. An initial coast followed by a tangential departure from the constraint boundary is a feasible solution. Figure 9 shows the geometry for an initial coast.

The imposed constraints are as follows:

$$\psi_1 = t_0 - t_1 \le 0 \tag{41}$$

$$\psi_2 = \boldsymbol{r}_1 - \boldsymbol{r}^{\#}(t_1) = \boldsymbol{0} \tag{42}$$

$$\psi_3 = -\boldsymbol{r}_1^T\boldsymbol{v}_1^+ \le 0 \tag{43}$$

where t_1 is the impulse time and $\boldsymbol{r}^{\#}(t)$ is the initial orbit of the spacecraft. The necessary conditions for an optimal solution are

$$\dot{\boldsymbol{p}}_1^+ = \dot{\boldsymbol{p}}_1^- - \lambda_2 + \lambda_3\left(\boldsymbol{v}_1^+ - \boldsymbol{M}_{f1}^T\boldsymbol{N}_{f1}^{-T}\boldsymbol{r}_1\right) \tag{44}$$

$$H_1^+ = H_1^- - \lambda_2^T\boldsymbol{v}^{\#}(t_1) + \lambda_3\boldsymbol{r}_1^T\left(\boldsymbol{g}_1 + \boldsymbol{N}_{f1}^{-1}\boldsymbol{M}_{f1}\boldsymbol{v}_1^+\right) - \lambda_1 \tag{45}$$

and Kuhn-Tucker conditions of the form of Eq. (26) also apply for λ_1 and λ_3. It is clear that the equality constraint of Eq. (42) introduces

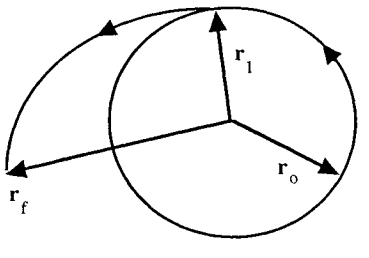

Fig. 9 Initial coast on the circular constraint boundary.

discontinuities in the primer vector rate and the Hamiltonian at the impulse time t_1.

The discussion and analysis that follow apply equally well for a final coast in orbital rendezvous. In fact, an optimal solution with time running backwards is also an optimal solution, due to the absence of dissipative effects, and an initial coast then becomes a final coast. However, this time reversal symmetry is broken in orbital interception due to the lack of symmetry in the terminal boundary conditions.

It is of interest to compare the initial coast (ic) solution with the optimal three-impulse periapse-constrained solution, which leaves the constraint boundary at the initial time and subsequently skims the boundary. Two rendezvous solutions and two interception solutions are given next. In all cases the initial vehicle velocity is (0, 1, 0) and the target is in circular orbit. The reference cost cited violates the minimum-radius constraint.

For a rendezvous with $T = 5.0$:

$$r_0 = (1, 0, 0) \qquad r_f = (-1.961329, -0.391398, 0)$$

$$J_{\text{ref}} = 0.401024 \qquad \dot{p}_0 = 0.454165$$

$$J_{\text{ic}} = 0.361255 \qquad J_3 = 0.360635$$

For a rendezvous with $T = 4.5$:

$$r_0 = (1, 0, 0) \qquad r_f = (-1.961329, -0.391398, 0)$$

$$J_{\text{ref}} = 0.524765 \qquad \dot{p}_0 = 0.185601$$

$$J_{\text{ic}} = 0.493291 \qquad J_3 = 0.490705$$

For an interception with $T = 5.0$:

$$r_0 = (1, 0, 0) \qquad r_f = (-1.961329, -0.391398, 0)$$

$$J_{\text{ref}} = 0.224455 \qquad \dot{p}_0 = 0.57376$$

$$J_{\text{ic}} = 0.167516 \qquad J_3 = 0.167509$$

For an interception with $T = 4.5$:

$$r_0 = (1, 0, 0) \qquad r_f = (-1.961329, -0.391398, 0)$$

$$J_{\text{ref}} = 0.287073 \qquad \dot{p}_0 = 0.411196$$

$$J_{\text{ic}} = 0.197608 \qquad J_3 = 0.197602$$

In all the given cases the cost of the three-impulse periapse-constrained solution is lower than the initial coast solution. Furthermore, the primer magnitude is greater than unity on the initial coast arc, indicating that the initial coast arc is nonoptimal, in general. An explanation for this fact is that for an initial coast, the vehicle trajectory is constrained to lie along the initial orbit until the vehicle can leave tangentially. Relaxing this equality constraint results in a solution of lower cost.

Bifurcation Solutions

An interesting and unexpected bifurcation phenomenon can occur in the optimal constrained rendezvous solution. For symmetric boundary conditions, symmetric optimal solutions are expected and are found for sufficiently small transfer times. However as the transfer time is increased to some critical value, some of the extremal solutions become nonsymmetric and nonunique. The single symmetric extremal solution splits into two nonsymmetric ones.

An example of this phenomenon is a rendezvous between circular orbits for which the boundary conditions are symmetric about the y-axis,

$$r_0 = (0.813173, -0.813173, 0)$$

$$r_f = (-0.813173, -0.813173, 0)$$

The path constraint is a maximum-radius constraint with $r_{\text{mx}} = 1.2$ with the initial and final circular orbits having equal radii of magnitude 1.15. For a sufficiently small transfer time the optimal solution is symmetric as expected. The optimal solution utilizes five impulses.

$$T = 6.15 \qquad J_5 = 0.0943968$$

$$t_1 = 0 \qquad r_1 = r_0$$

$$t_2 = 2.5597 \qquad r_2 = (0.452559, 1.11065, 0)$$

$$t_3 = 3.0750 \qquad r_3 = (0, 1.19947, 0)$$

$$t_4 = 3.5903 \qquad r_4 = (-0.452559, 1.11605, 0)$$

$$t_5 = 6.15 \qquad r_5 = r_f$$

Note that the times all of the impulses are symmetric about the half-transfer time. Also, the impulse locations are symmetric about the y axis.

However, as the transfer time is increased this symmetry breaks down. For a larger transfer time the optimal solution utilizes eight impulses but the five-impulse extremal solution is given by

$$T = 7.2 \qquad J_5 = 1.66287$$

$$t_1 = 0 \qquad r_1 = r_0$$

$$t_2 = 1.20426 \qquad r_2 = (1.12384, -0.108944, 0)$$

$$t_3 = 2.30162 \qquad r_3 = (1.03807, 0.44514, 0)$$

$$t_4 = 3.45369 \qquad r_4 = (0.565045, 1.0116, 0)$$

$$t_5 = 7.2 \qquad r_5 = r_f$$

Note that the impulse times t_k are not symmetric about the half-transfer time. Also notice that, by symmetry of the boundary conditions, a second nonsymmetric solution of the same cost exists if one mirror reflects the r_k across the y-z plane and replaces T by $T - t_k$. The extremal solution is, therefore, nonunique and, a bifurcation has occurred. None of the impulses lies on the maximum-radius constraint boundary. The constraint becomes active as the trajectory passes through apoapse at a time between impulses. A physical explanation for this nonsymmetric solution is not known to the authors.

Singular Arc Solutions

Consider the special case of starting at rest on a minimum-radius circular constraint boundary. A physical example of this would be a vehicle on the surface of a planet or moon. If the two-impulse rendezvous or one-impulse intercept trajectory violates the path constraint, one feasible solution is to use the first impulse to orbit along the circular constraint boundary, followed by an additional impulse to leave the boundary and fly to the target. This boundary arc is a singular arc[1] with the constant magnitude primer vector equal to the velocity vector along the circular orbit. An alternative trajectory is a three- or four-impulse periapse-constrained solution of the type considered previously.

Surprisingly, in all cases investigated the singular arc solution was nonoptimal. As seen in the numerical results that follow, the difference in cost on the optimal solution, for which only the periapses touch the constraint boundary, is quite small. However, because the calculations were done in double precision (15 decimal digits accuracy) on a Convex 220 mainframe, the numerical results are considered trustworthy.

In all cases $v_0 = (0, 0, 0)$ and the initial point lies on the constraint boundary of unit radius. The reference cost cited is the two-impulse (rendezvous) or one-impulse (intercept) solution that violates the constraint. For the rendezvous solutions the target is in a circular orbit of radius 1.2.

For a rendezvous with $T = 4.0$:

$$r_0 = (0.866025, -0.5, 0) \qquad r_f = (-1.2, 0, 0)$$

$$J_{\text{ref}} = 1.09113 \qquad v_f = (0, -0.912871, 0)$$

$$J_{\text{singular}} = 1.10422 \qquad J_3 = 1.10414$$

For a rendezvous with $T = 3.3$:

$$\boldsymbol{r}_0 = (0.996195, 0.087156, 0) \qquad \boldsymbol{r}_f = (-1.2, 0, 0)$$

$$J_{\text{ref}} = 1.115861 \qquad \boldsymbol{v}_f = (0, -0.912871, 0)$$

$$J_{\text{singular}} = 1.13516 \qquad J_3 = 1.13396$$

For an interception with $T = 5.0$:

$$\boldsymbol{r}_0 = (0.996195, 0.087156, 0) \qquad \boldsymbol{r}_f = (-1.2, 0, 0)$$

$$J_{\text{ref}} = 1.046777 \qquad \boldsymbol{v}_f = (0, -0.912871, 0)$$

$$J_{\text{singular}} = 1.05304 \qquad J_4 = 1.052976$$

In the last case the optimal, four-impulse periapse-constrained solution is cited. It is interesting to note that the cost for the nonoptimal three-impulse periapse-constrained solution is 1.05302, which, although higher than the optimal cost, is still less than the singular arc cost.

Conclusions

Optimal impulsive trajectories have been investigated for the case of path constraints in an inverse-square gravitational field. As shown by the simple case of a minimum-radius path constraint in field-free space, interior path constraints significantly increase the complexity of an optimal impulsive rendezvous or interception trajectory. Primer vector theory has been extended to incorporate various types of interior path constraints. The use of a periapse or apoapse constraint for a conic orbit is found to be workable to implement a minimum- or maximum-radius constraint.

One distinguishing feature of the impulsive path-constrained problem is that the Hamiltonian function is, in general, discontinuous at a midcourse impulse, even when the impulse time is unspecified. This is in contrast to the impulsive thrust problem without path constraints, in which the Hamiltonian is discontinuous only if the midcourse impulse time is constrained, i.e., a rheonomic rather than scleronomic constraint.

A major conclusion from this study is that the constrained optimal impulsive solution consists of isolated boundary points only. Even though a circular boundary arc is a possible coast arc between impulses, it does not, in general, constitute a part of an optimal solution. The constrained optimal trajectory is tangent to the boundary only at isolated points. The savings in cost achieved by the periapse-constrained solutions compared with boundary arcs is significant.

Initial and final coast arcs represent equality path constraints, and a lower cost can often be realized by relaxing this type of constraint. The use of an additional impulse can typically result in a lower cost. Because terminal coast arcs represent path constraints, the primer vector rate and the Hamiltonian are typically discontinuous entering or leaving a terminal coast.

An interesting bifurcation phenomenon can occur in the case of rendezvous with a maximum-radius constraint. As the transfer time is increased, the symmetric optimal solution for symmetric boundary conditions bifurcates into two nonsymmetric extremal solutions having equal cost. A physical explanation of this phenomenon is not known to the authors.

Singular arcs on the constraint boundary have been observed to be nonoptimal even though they satisfy the necessary conditions. They represent suboptimal solutions compared with periapse-constrained optimal solutions. The savings in cost achieved by the periapse-constrained optimal solutions in these cases is quite small.

Acknowledgment

This research was supported in part by the NASA Lewis Research Center through NASA Grant NAG 3-1138.

References

[1]Lawden, D. F., *Optimal Trajectories for Space Navigation*, Butterworths, London, 1963.

[2]Lion, P. M., and Handelsman, M., "Primer Vector on Fixed-Time Impulsive Trajectories," *AIAA Journal*, Vol. 6, No. 1, 1968, pp. 127–132.

[3]Gobetz, F. W., and Doll, J. R., "A Survey of Impulsive Trajectories," *AIAA Journal*, Vol. 7, No. 5, 1969, pp. 801–834.

[4]Gross, L. R., and Prussing, J. E., "Optimal Multiple-Impulse Direct Ascent Fixed-Time Rendezvous," *AIAA Journal*, Vol. 12, No. 7, 1974, pp. 885–889.

[5]Prussing, J. E., and Chiu, J.-H., "Optimal Multiple-Impulse Fixed-Time Rendezvous Between Circular Orbits," *Journal of Guidance, Control, and Dynamics*, Vol. 9, No. 1, 1986, pp. 17–22.

[6]Prussing, J. E., Wellnitz, L. J., and Heckathorn, W. G.,"Optimal Impulsive Time-Fixed Direct-Ascent Interception," *Journal of Guidance, Control, and Dynamics*, Vol. 12, No. 4, 1989, pp. 487–494.

[7]Jezewski, D. J., and Faust, N. L., "Inequality Constraints in Primer-Optimal N-Impulse Solutions," *AIAA Journal*, Vol. 9, No. 4, 1971, pp. 760–763.

[8]Jezewski, D. J., "Primer Vector Theory and Applications," NASA TR R-454, Nov. 1975.

[9]Brusch, R. G., "Constrained Impulsive Trajectory Optimization for Orbit-to-Orbit Transfer," *Journal of Guidance, Control, and Dynamics*, Vol. 2, No. 3, 1979, pp. 204–212.

[10]Stern, S. A., and Fowler, W. T., "Path-Constrained Maneuvering Near Large Space Structures," *Journal of Spacecraft and Rockets*, Vol. 22, No. 5, 1985, pp. 548–553.

[11]Soileau, K. M., and Stern S. A., "Path-Constrained Rendezvous: Necessary and Sufficient Conditions," *Journal of Spacecraft and Rockets*, Vol. 23, No. 5, 1986, pp. 492–498.

[12]Prussing, J. E., and Clifton, R. S., "Optimal Multiple-Impulse Satellite Evasive Maneuvers," *Journal of Guidance, Control, and Dynamics*, Vol. 17, No. 3, 1994, pp. 599–606.

[13]Taur, D. R., "Optimal, Impulsive, Time-Fixed Orbital Rendezvous and Interception with Path Constraints," Ph.D. Thesis, Univ. of Illinois at Urbana-Champaign, IL, 1989.

[14]Battin, R. H., *Introduction to the Mathematics and Methods of Astrodynamics*, AIAA Education Series, AIAA, 1987.

[15]Prussing, J. E., and Conway, B. A., *Orbital Mechanics*, Oxford Univ. Press, 1993.